Multiqubit entanglement in bidirectional-chiral-waveguide QED

Imran M. Mirza
Department of Physics, University of Michigan, Ann Arbor, Michigan 48109, USA

John C. Schotland
Department of Mathematics and Department of Physics, University of Michigan, Ann Arbor, Michigan 48109, USA

(Received 29 February 2016; published 1 July 2016)

We study the generation of transient entanglement induced by a single-photon Gaussian wave packet in multiatom bidirectional-waveguide QED. In particular, we investigate the effect of increasing the number of atoms on the average pairwise entanglement. We demonstrate, by selecting smaller decay rates and in chiral-waveguide settings, that both entanglement survival times and maximum generated entanglement can be increased by at least a factor of $\sim 3/2$, independent of the number of atoms. In addition, we analyze the influence of detuning and delays on the robustness of the generated entanglement. There are potential applications of our results in entanglement-based multiqubit quantum networks.

DOI: 10.1103/PhysRevA.94.012302

I. INTRODUCTION

Quantum circuits are envisioned to play an indispensable role in the physical implementation of quantum computers [1]. In optical quantum computing and in several quantum information processing protocols, controlled light-matter interactions are an essential requirement [2,3]. Two principal setups have been proposed to achieve such interactions: cavity QED and waveguide QED systems. In cavity QED [4], matter in the form of qubits interacts with one or a few discrete optical modes confined within an optical resonator. At the same time, atoms can strongly couple with cavity modes, thereby producing well-known phenomena such as Rabi oscillations [5]. In contrast, in waveguide QED [6,7], qubits interact with flying photons which propagate through infinitely many waveguide modes. Such configurations may serve as longer input-output quantum networks. In both types of systems, atom-light interactions can generate qubit-qubit and qubit-photon entanglement, which is a necessary resource for performing many key tasks in quantum information processing and quantum computing.

Waveguide-based structures are proving to be excellent platforms for quantum circuits. Some appealing examples in this regard are plasmonic waveguides [8], photonic crystals [9,10], superconducting circuits [11], and optical lattices [12]. In previous waveguide QED studies, two-qubit entanglement generation has been analyzed when either an input coherent field or a single photon (produced through an excited qubit) serves as a qubit-qubit entanglement agent [13–15]. We note that in the context of cavity QED systems, single-photon input-output-based stationary entanglement generation schemes have also been proposed [16,17]. However, an actual quantum network will, in general, require multiple qubits, wherein flying photons will serve as information carriers. In this setting, qubits become entangled at specified nodes in the network.

Motivated by the above considerations, in this paper we study the impact of increasing the number of atoms on single-photon multiqubit entanglement in bidirectional waveguide QED structures. Note that in order to establish stationary entanglement among qubits (which is more useful for multiqubit entanglement-based quantum networks), one can employ so-called driven dissipative methods, in which photon decay is correctly balanced with the aid of an input coherent drive. See Refs. [18,19] for the application of these methods in waveguide QED and cavity QED systems, respectively. In contrast, in this work we investigate how (without a constant coherent drive) flying qubits can transiently entangle waveguide-coupled stationary qubits and how such transient entanglement can be stored for prolonged times. The theoretical model we consider is relevant to recent developments in the subject of photonic interactions with a one-dimensional qubit array, mainly in circuit QED and photonic crystal waveguide systems [9,20,21]. We focus specifically on the question of how system parameters can be engineered to control waveguide-mediated qubit-qubit entanglement. As opposed to choosing a fixed atom as a single-photon source [14], here we consider the situation in which a single-photon Gaussian wave packet serves as both an input drive and an entanglement generator. To this end, we derive and then utilize a single-photon bidirectional Fock-state master equation.

The three main approaches used in waveguide QED to study scattering of photons and entanglement are the real-space formalism [22], the input-output formalism [23,24], and other master-equation approaches [14,25]. The main novelty of using the Fock-state master equation relies on the fact that it both captures the qubit dynamics and keeps track of the state of the reservoirs at the same time due to its non-Markovian structure. Using this approach, we first study the effect of increasing the number of atoms on the pairwise concurrence. We find that the entanglement survival time markedly decreases. We also find that the maximum concurrence decreases by a factor of $\sim 1/20$ as the number of atoms increases from two to five. However, we demonstrate that small decay rate and chirality can resolve these issues. In addition, we introduce a finite detuning between the peak frequency of the incoming single-photon wave packet and the atomic transition frequency. We notice that in comparison to the on-resonance case, detuning does not affect the overall temporal profile of the entanglement, but the maximum concurrence is reduced. Furthermore, when

interatomic delays are incorporated, we observe, independent of N, that smaller delays support an overall larger pairwise concurrence. Moreover, characteristic patterns of death and revival of entanglement appear.

The remainder of this paper is organized as follows. In Sec. II we introduce the details of the system and its dissipative dynamics. In Sec. III we report our results. Finally, in Sec. IV we close by summarizing our conclusions. In the Appendix, we outline the derivation of the bidirectional master equation that is our main tool in this work.

II. THEORETICAL DESCRIPTION

A. Setup

The system under consideration consists of a chain of two-level emitters (atoms, quantum dots, artificial atoms, or nitrogen-vacancy centers in diamond [26–29]) side coupled to a dispersionless and lossless waveguide (see Fig. 1). The frequency of the ground state $|g_i\rangle$ and excited state $|e_i\rangle$ of the ith atom in the chain is denoted by ω_{g_i} and ω_{e_i} for $i = 1,\ldots,N$. The process of deexcitation of the ith atom is described by the atomic lowering operator $\hat{\sigma}_i = |g_i\rangle\langle e_i|$. All atoms are coupled to a common waveguide which has two continua of modes: a left-moving continuum and a right-moving continuum. Destruction of a single photon in the left- (right-) moving continuum is described by the annihilation operator $\hat{b}_L(\omega_2)$ [$\hat{b}_R(\omega_2)$]. The waveguide continua are treated as two reservoirs or baths. We will assume that, initially, the right-moving reservoir is in a single-photon pure state $|\Psi_{\mathcal{R}_1}\rangle$, while the left-moving reservoir is in the vacuum state, with $|\Psi_{\mathcal{R}_2}\rangle = |\text{vac}\rangle$. The explicit form of $|\Psi_{\mathcal{R}_1}\rangle$ is given by

$$|\Psi_{\mathcal{R}_1}\rangle = \int_0^\infty g(\omega_1)\hat{b}_R^\dagger(\omega_1)|\text{vac}\rangle d\omega_1, \tag{1}$$

where $g(\omega_1)$ represents the spectral profile of the single-photon wave packet. Note that the normalization condition on $|\Psi_{\mathcal{R}_1}\rangle$ requires that $\int_0^\infty |g(\omega_1)|^2 d\omega_1 = 1$. The nonvanishing commutation relations among operators describing the system are given by

$$\begin{aligned}[\hat{b}_R(\omega_1),\hat{b}_R(\omega_1')] &= \delta(\omega_1-\omega_1'),\\ [\hat{b}_L(\omega_2),\hat{b}_L(\omega_2')] &= \delta(\omega_2-\omega_2'),\\ [\hat{\sigma}_i^\dagger,\hat{\sigma}_j] &= \hat{\sigma}_{zi}\delta_{ij},\end{aligned} \tag{2}$$

where $\hat{\sigma}_{zi} = |e_i\rangle\langle e_i| - |g_i\rangle\langle g_i|$.

B. Dissipative dynamics and bidirectional Fock-state master equation

The system shown in Fig. 1 is an open quantum system due to the interaction of the atoms with the waveguide continua. However, the dissipative dynamics of the system cannot be described by traditional Born-Markov master equations (Lehmberg type) [30,31]. This follows from the fact that once a single photon is absorbed by one of the atoms in the chain, the state of the right-moving reservoir changes, which may introduce non-Markovian effects. In view of this observation, we rederive the single-photon Fock-state master equation, which describes the bidirectional coupling between atoms, accounting for decoherence effects. The derivation is outlined in the Appendix. We thus obtain the following master equation for the evolution of the system density operator $\hat{\rho}_s$:

$$\begin{aligned}\frac{d\hat{\rho}_s(t)}{dt} &= \hat{\mathcal{L}}_{cs}[\hat{\rho}_s(t)] + \hat{\mathcal{L}}_{pd}[\hat{\rho}_s(t)] + \hat{\mathcal{L}}_{cd}[\hat{\rho}_s(t)]\\ &\quad + \sum_{i=1}^{N}\sqrt{2\gamma_{iR}}\{e^{ik_0d_i}g(t)[\hat{\rho}_{01}(t),\hat{\sigma}_i^\dagger]\\ &\quad + e^{-ik_0d_i}g^*(t)[\hat{\sigma}_i,\hat{\rho}_{10}(t)]\}.\end{aligned} \tag{3}$$

Here for any density operator $\hat{\varrho}(t)$, the action of the aforementioned Liouvillian superoperators is given by

$$\hat{\mathcal{L}}_{cs}[\hat{\varrho}(t)] = -\frac{i}{\hbar}[\hat{H}_{\text{sys}},\hat{\varrho}(t)], \hat{H}_{\text{sys}} = \hbar\sum_{i=1}^{N}\Delta_i\hat{\sigma}_i^\dagger\hat{\sigma}_i,$$

$$\hat{\mathcal{L}}_{pd}[\hat{\varrho}(t)] = -\sum_{i=1}^{N}\gamma_{iRL}[\hat{\sigma}_i^\dagger\hat{\sigma}_i\hat{\varrho}(t) - 2\hat{\sigma}_i\hat{\varrho}(t)\hat{\sigma}_i^\dagger + \hat{\varrho}(t)\hat{\sigma}_i^\dagger\hat{\sigma}_i],$$

$$\begin{aligned}\hat{\mathcal{L}}_{cd}[\hat{\varrho}(t)] &= -\sum_{i\neq j=1}^{N}(\sqrt{\gamma_{iR}\gamma_{jR}}\delta_{i>j} + \sqrt{\gamma_{iL}\gamma_{jL}}\delta_{i<j})\\ &\quad\times\{[\hat{\sigma}_j^\dagger\hat{\sigma}_i\hat{\varrho}(t) - \hat{\sigma}_i\hat{\varrho}(t)\hat{\sigma}_j^\dagger]e^{-2\pi iD(i-j)}\\ &\quad - [\hat{\sigma}_j\hat{\varrho}(t)\hat{\sigma}_i^\dagger - \hat{\varrho}(t)\hat{\sigma}_i^\dagger\hat{\sigma}_j]e^{2\pi iD(i-j)}\},\end{aligned}$$

where $g(t)$ is the temporal profile of the wave packet obtained by Fourier transformation of $g(\omega_1)$ and $\Delta_i = \omega_{egi} - \omega_p$ is the detuning between ω_{egi} and the peak frequency ω_p of the single-photon input drive. The parameters γ_{iL} and γ_{iR} are

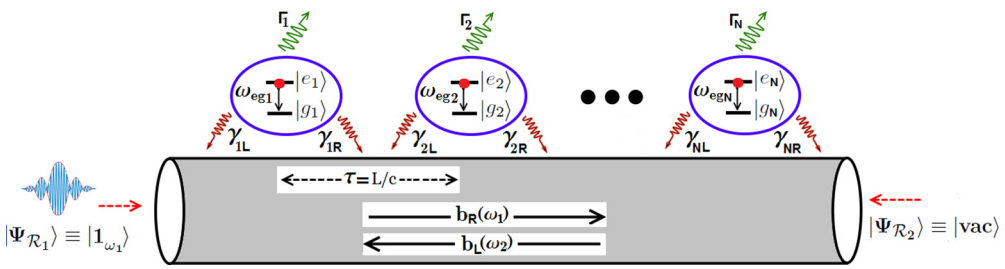

FIG. 1. Illustration of a single-photon wave packet driving a system of N two-level atoms side coupled to a waveguide. Any two consecutive atoms are separated by the distance L (or time delay $\tau = L/v_g$, with $v_g = c$ being the group velocity of a single photon in the waveguide). Two-mode waveguide continua serve as channels for the wave packet to propagate through. The atom-waveguide coupling causes atoms to be excited but also generates qubit-qubit entanglement. The quantity Γ_i is the emission rate of the ith atom into the free-space channel; such decays are ignored in the present analysis. Consequently, the coupling fraction parameter [14] $\beta_i = (\gamma_{iL} + \gamma_{iR})/(\gamma_{iL} + \gamma_{iR} + \Gamma_i)$ has been set equal to unity throughout this paper.

the spontaneous emission rates of the ith atom to decay into the left- and right-moving waveguide continua, respectively, and $\gamma_{iRL} = (\gamma_{iR} + \gamma_{iL})/2$. We also define $k_0 = \omega_{eg}/v_g$ to be the wave number of the waveguide-emitted photon. Finally, d_i specifies the position of the ith atom such that $D(i-j) = 2\pi(d_i - d_j)k_0$. The first term on the right-hand side of (3) (with subscript cs) describes the closed-system dynamics, the second term (with subscript pd) represents the pure decay of energy from the atoms into the waveguide continua, and the terms multiplied with $\sqrt{\gamma_{iR}\gamma_{jR}}$ and $\sqrt{\gamma_{iL}\gamma_{jL}}$ (terms with subscript cd) are the cooperative decay terms (with $j = 1,2,3,\ldots,N$). The operator $\hat{\rho}_{10}$, which appears in (3), is defined as

$$\hat{\rho}_{10}(t) = \mathrm{Tr}_R[\hat{U}(t-t_0)\hat{\rho}_s(t)|\mathrm{vac}\rangle\langle\Psi_{\mathcal{R}_1}|\hat{\rho}_{\mathcal{R}_2}(t_0)\hat{U}^\dagger(t-t_0)],$$

which obeys the equation of motion

$$\frac{d\hat{\rho}_{10}(t)}{dt} = \hat{\mathcal{L}}_{cs}[\hat{\rho}_{10}(t)] + \hat{\mathcal{L}}_{pd}[\hat{\rho}_{10}(t)] + \hat{\mathcal{L}}_{cd}[\hat{\rho}_{10}(t)] + \sum_{i=1}^{N}\sqrt{2\gamma_{iR}}e^{-ik_0d_i}g^*(t)[\hat{\rho}_{00}(t),\hat{\sigma}_i^\dagger]. \quad (4)$$

Here

$$\hat{\rho}_{00}(t) = \mathrm{Tr}_R[\hat{U}(t-t_0)\hat{\rho}_s(t)|\mathrm{vac}\rangle\langle\mathrm{vac}|\hat{\rho}_{\mathcal{R}_2}(t_0)\hat{U}^\dagger(t-t_0)]$$

obeys the no-drive (or vacuum) Lehmberg master equation

$$\frac{d\hat{\rho}_{00}(t)}{dt} = \hat{\mathcal{L}}_{cs}[\hat{\rho}_{00}(t)] + \hat{\mathcal{L}}_{pd}[\hat{\rho}_{00}(t)] + \hat{\mathcal{L}}_{cd}[\hat{\rho}_{00}(t)]. \quad (5)$$

In Eq. (5) $\hat{\rho}_{\mathcal{R}_2}(t_0)$ is the initial vacuum state of the second reservoir, and $\hat{U}(t-t_0)$ is the time evolution operator of the global (qubits plus reservoirs) system. It is worthwhile to note that unlike the usual non-Markovian master equations in which time-dependent decay rates and frequency shifts carry the memory effects [32,33], the single-photon Fock-state master equation [Eq. (3)] we derived is also non-Markovian, but from a different point of view. The non-Markovian property is due to the appearance of a novel $\hat{\rho}_{01}(t)$ density operator in Eq. (3), which carries information about the change in the reservoir state after the absorption of a single photon. Note that, following the idea of the Markov approximation, the Markovian master equation does not keep track of changes in the state of the reservoirs.

In their study of a continuous-mode $\mathcal{N}$-photon wave packet interacting with a quantum system, Baragiola *et al.* have derived a similar master equation for the case $\mathcal{N} = 1$ [34]. In their work, they utilized the machinery of quantum stochastic differential equations. We note that the main novelty of our master equation (3) relies on its bidirectional nature, which is more suitable for waveguide QED problems. Equations (3), (4), and (5) provide a set of equations needed to obtain a closed-form solution for the system density operator $\hat{\rho}_s(t)$.

III. RESULTS AND DISCUSSION

In principle, we can use the bidirectional single-photon Fock-state master equation to calculate any observable of interest. In what follows, we will concentrate on how the incident single photon populates the atomic chain, with the concomitant generation of entanglement. In particular, we will study the evolution of measures of entanglement and the influence of bidirectional-waveguide-mediated coupling.

A. Influence of the number of atoms on population transfer and pairwise entanglement

For the remainder of this paper, we assume that the temporal shape of the single-photon wave packet is a Gaussian function of time of the form

$$g(t) = \frac{1}{\sqrt{2\pi}\Delta t}e^{-(t-\bar{t})^2/2(\Delta t)^2}, \quad (6)$$

where $\bar{t}$ and Δt are the mean and width of the Gaussian. Next, as an initial condition, we take all atoms to be in their ground state. That is, $\hat{\rho}_s(t_0) = |G\rangle\langle G|$, $\hat{\rho}_{00}(t_0) = |G\rangle\langle G|$, and $\hat{\rho}_{10}(t_0) = 0$ for some initial time t_0, where $|G\rangle$ denotes the state in which all atoms occupy their ground state. We also denote by $|E_1\rangle$ the state where any one of the atoms is excited. We first calculate the probability $P_i^{(1)}(t) = \mathrm{Tr}[\hat{\rho}_s(t)|E_1\rangle\langle E_1|]$ that any one of the atoms in the chain is excited for $i = 1,2,\ldots,5$. We also calculate the corresponding probability that all atoms are in the ground state, denoted $P_i^{(G)}(t) = \mathrm{Tr}[\hat{\rho}_s(t)|G\rangle\langle G|]$. The main focus of this section will be to investigate how increasing the number of atoms in the chain impacts these probabilities.

Under the above initial conditions and for a single atom in the chain, we obtain a closed-form expression for the excitation probability $P_1^{(1)}(t)$. To this end, we assume that a single atom is initially unexcited, and as an advantageous consequence, we observe from Eq. (5) that $\hat{\rho}_{00}(t)$ does not evolve in time, i.e.,

$$\hat{\rho}_{00}(t) = e^{\hat{\mathcal{L}}(t-t_0)}\hat{\rho}_{00}(t_0) = \sigma\sigma^\dagger, \quad (7)$$

where $\hat{\mathcal{L}}[\hat{\varrho}(t)] = \hat{\mathcal{L}}_{cs}[\hat{\varrho}(t)] + \hat{\mathcal{L}}_{pd}[\hat{\varrho}(t)] + \hat{\mathcal{L}}_{cd}[\hat{\varrho}(t)]$. We can then integrate Eq. (4) to obtain

$$\hat{\rho}_{01}(t) = -\int_{t_0}^{t}\Omega^*(t')e^{(i\omega_{eg}-\gamma)(t-t')}\hat{\sigma}\,dt', \quad (8)$$

where $\Omega(t) \equiv \sqrt{2\gamma_{1R}}g(t)$. Inserting the above solution into Eq. (3), we find the required atom density operator:

$$\hat{\rho}_s(t) = \hat{\rho}_s(t_0) + [\hat{\sigma}^\dagger,\hat{\sigma}]\int_{t_0}^{t}\int_{t_0}^{t'}\Omega(t',t'')e^{-2\gamma(t-t')}dt'dt'', \quad (9)$$

where $\Omega(t,t') = 2\mathrm{Re}[\Omega(t)\Omega^*(t')e^{(i\omega_{eg}-\gamma)(t-t')}]$. To proceed further, we express the temporal profile of the single-photon wave packet as $\Omega(t) = \mu(t)e^{i\omega_p(t)}$, where $\mu(t)$ is assumed to be slowly varying on the time scale of γ^{-1} and is related to $g(t)$ through $\mu(t) = \sqrt{2\gamma_{1R}}|g(t)|$. Carrying out the above integral, we obtain

$$\hat{\rho}_s(t) \simeq \hat{\rho}_s(t_0) + \left(\frac{2\gamma|g(t)|^2}{(\omega_{eg}-\omega_p)^2+\gamma^2}\right)[\hat{\sigma}^\dagger,\hat{\sigma}]. \quad (10)$$

Utilizing this result [35], the quantity $P_1^{(1)}(t)$ can then be obtained.

Along with the population dynamics, we will also study the generation and evolution of qubit-qubit entanglement. For the entanglement calculations, we begin with the two-atom chain. For such a bipartite mixed state, the concurrence $C(\hat{\rho}_s)$ is a useful measure of entanglement [36]. Following Wootters, we

define the concurrence $C(t)$ as

$$C(t) = \max(0, \sqrt{\lambda_1} - \sqrt{\lambda_2} - \sqrt{\lambda_3} - \sqrt{\lambda_4}), \qquad (11)$$

where λ_i are the eigenvalues (in descending order) of the spin-flipped density matrix $\widetilde{\rho}_s = \hat{\rho}_s(\hat{\sigma}_y \otimes \hat{\sigma}_y)\hat{\rho}_s^*(\hat{\sigma}_y \otimes \hat{\sigma}_y)$, with $\hat{\sigma}_y$ being the Pauli spin-flip operator. The upper and lower bounds on the concurrence are 1 and 0, respectively. We note that $C = 1$ corresponds to a maximally entangled state (for instance, Bell or Einstein-Podolsky-Rosen states), while $C = 0$ corresponds to an unentangled state. For the case of more than two atoms, we will employ the pairwise average concurrence [37–40], defined as $\mathcal{C}(t) = [\sum_{i=1}^{n} C_i(t)]/n$, where $n = N/2$ is the total number of pairs of atoms in the chain. We note that this definition of concurrence has the same properties as each of the individual pair concurrences. We also point out that $\mathcal{C}(t)$ does not quantify the real multiqubit entanglement in the system; rather, it only measures pairwise entanglement. However, one can use other entanglement measurements, such as spin squeezing [18], to quantify multiqubit entanglement. In principle, from the master equations we derive, it is possible to calculate the spin-squeezing parameter. We direct the reader to Ref. [41], where for multiqubit states the relation between the spin-squeezing parameter and pairwise entanglement has been investigated.

We now return to our numerical results. In Fig. 2, we plot the single-excitation population dynamics and the temporal profile of the entanglement. We find that a single atom in the chain can be excited with probability $P_1^{(1)}$ up to 35%. This probability remains to one third of its maximum value at the time ($t \sim 7\gamma^{-1}$) when the single-photon pulse vanishes. It takes a further time $t = \gamma^{-1}$ for $P_1^{(1)}$ to vanish completely. This value of $P_1^{(1)}$ is less than half of what is reported for a single-photon Gaussian input state that is on resonance [42]. The difference can be attributed to the presence of bidirectional decays in our model. As the number of atoms in the chain increases, we note that the maximum value of the population decreases. In particular, for the cases of two, three, four, and five atoms in the chain, the maximum population drops down to 24%, 18%, 14%, and 11%, respectively. Moreover, the temporal shape of the excited-state populations $P_k^{(1)}$ is symmetric about the maximum value induced by the drive.

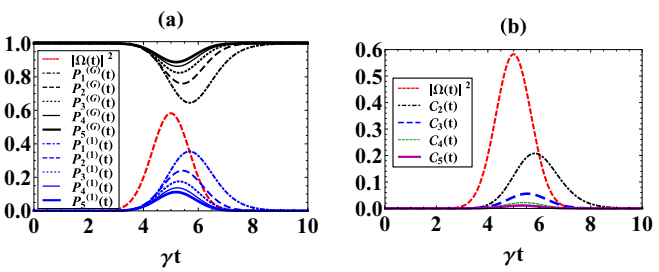

FIG. 2. Time evolution of (a) populations and (b) entanglement as quantified by pairwise concurrence for a system of up to a five-atom chain in a waveguide QED setup. A single-photon wave packet [$\Omega(t) = \sqrt{2\gamma}g(t)$] with mean value $5\gamma^{-1}$ and width $1.5\gamma^{-1}$ drives the system strongly ($|\Omega|_{\max} > \gamma$) from the right-hand side. An on-resonance situation is considered with $\omega_{eg} = \omega_p$ (ω_{eg} is the transition frequency of the atoms). For simplicity, all decay rates (pure and cooperative) are assumed to be equal: $\gamma_{iL} = \gamma_{iR} = \gamma$. The single-photon wave-packet parameters are chosen to achieve the maximum value of the single excitation in the system [42]. We see that increasing the number of qubits in the system leads to decreases in both population transfer and net entanglement.

For entanglement calculations, we begin with the case of two-qubit concurrence. The spin-flip density matrix in this case takes the following form:

$$\widetilde{\rho}_s(t) = \begin{pmatrix} |\rho_1|^2 & 0 & 0 & \rho_1^*\rho_4 \\ 0 & |\rho_6|^2 + |\rho_7|^2 & |\rho_6|^2 + |\rho_7|^2 & 0 \\ 0 & |\rho_{10}|^2 + |\rho_{11}|^2 & |\rho_{10}|^2 + |\rho_{11}|^2 & 0 \\ 0 & 0 & 0 & 0 \end{pmatrix}, \qquad (12)$$

where $\rho_1 = \langle g_1 g_2|\hat{\rho}_s|g_1 g_2\rangle, \rho_4 = \langle g_1 g_2|\hat{\rho}_s(t)|e_1 e_2\rangle$, $\rho_6 = \langle e_1 g_2|\hat{\rho}_s(t)|e_1 g_2\rangle, \rho_7 = \langle e_1 g_2|\hat{\rho}_s(t)|g_1 e_2\rangle$, $\rho_{10} = \langle g_1 e_2|\hat{\rho}_s(t)|e_1 g_2\rangle$, and $\rho_{11} = \langle g_1 e_2|\hat{\rho}_s(t)|g_1 e_2\rangle$. Here we employ the notation that the first (second) slot in the ket describes the state of the first (second) atom. We have observed numerically that various entries of $\widetilde{\rho}_s(t)$ vanish. We have verified this observation by directly integrating the equation of motion for $\hat{\rho}_{10}(t)$ using the fact that $\hat{\rho}_{00}(t)$ does not evolve in time if both atoms are initially in their ground states. To proceed, we inserted the obtained form of $\hat{\rho}_{10}(t)$ into (3). We found that up to fourth order in γ, only certain density matrix elements of $\hat{\rho}_s(t)$ which appear in (12) survive. Diagonalization of $\widetilde{\rho}_s(t)$ then yields the following set of eigenvalues:

$$\lambda_1 = 0, \quad \lambda_2 = 0, \quad \lambda_3 = |\rho_4|,$$
$$\lambda_4 = |\rho_6|^2 + |\rho_7|^2 + |\rho_{10}|^2 + |\rho_{11}|^2 = 4|\rho_c|^2 .$$

By numerical integration of (3), (4), and (5), we find that for a system of identical atoms driven by a symmetric Gaussian pulse $\rho_6 = \rho_7 = \rho_{10} = \rho_{11} = \rho_c$. Inserting these eigenvalues in (7), we obtain a rather compact form of the concurrence: $\mathcal{C}(t) = 2\rho_c - \rho_4$. We have plotted this form of the concurrence in Fig. 2(b).

We notice that even in the presence of pure and cooperative decays, an incoming single-photon wave packet generates entanglement between two qubits up to 20.8%. The entanglement takes $\sim\gamma^{-1}$ time to grow after the initial growth of the input drive. For the present choice of parameters, we find that the atoms remain entangled for a time $5\gamma^{-1}$. As the number of atoms is increased, the pairwise concurrence takes on smaller maximum values. As a result, for the cases of three, four, and five atoms, the pairwise concurrence attains the values 5.6%, 2.2%, and 1.1%, respectively. In addition, the entanglement survives for a corresponding time of (almost) $4\gamma^{-1}$,$3\gamma^{-1}$, and $2.5\gamma^{-1}$.

B. Entanglement storage and small decay rates

As pointed out above, if we increase the number of atoms in the chain, the entanglement is quickly lost. However, for certain quantum information processing protocols, the entanglement survival for prolonged times is one of the key requirements. See Refs. [43–45] and the applications mentioned therein. One straightforward way to accomplish this task is to isolate the system from the environment, that

is, by setting $\gamma_{iL} = \gamma_{iR} = 0$. However, such a choice comes at the price of diminishing qubit-qubit interactions in the system. This includes terms with the prefactor $\sqrt{\gamma_{iR}\gamma_{jR}}, \sqrt{\gamma_{iL}\gamma_{jL}}$ in Eq. (3), which influences entanglement generation and evolution. Keeping these points in mind, in the present section we consider the example of small decay rates. Such rates, for instance, can be obtained in an experiment exploiting reservoir engineering techniques [46,47]. Indeed, the smaller decay rates we consider here lie within the range of decay rates discussed in Refs. [14,48]. In Figs. 3(a) and 3(b), we consider small decay rates, which results in a longer survival of both the single-excitation populations and the pairwise concurrence among atoms. The highest values achieved by the population almost remain the same as those found in Fig. 2, but the entanglement tends to achieve a smaller maximum for a bipartite system. Moreover, the case of two atoms also shows the phenomenon of entanglement death and revival [49,50]. However, when three, four, or five atoms are included in the chain, the highest values of the entanglement for both small decay rates ($\tilde{\gamma} = 0.1\gamma$) and large decay rates (γ) almost match.

The survival times (in terms of the pulse duration time $\Delta t_D = 4.85\gamma^{-1}$) are plotted in Fig. 3(c) as a function of the number of atoms in the chain for the cases of both small and large decay. We find that as soon as we choose $\tilde{\gamma}$ as the decay rate, both population (Δt_p) and entanglement (Δt_C) survival times increase by a factor of 2 compared to a decay rate of γ. Another interesting feature in Fig. 3(c) is a jump in Δt_p and Δt_C as we move from two- to three-atom chains. This behavior seems to indicate that there is an optimal point between the extremes of pure decay and qubit-qubit coupling. In the case of three atoms in the chain, qubit-qubit coupling starts to dominate for smaller decay rates. In the four- and five-atom cases, decay mechanisms begin to overwhelm interatomic couplings, which results in the same behavior followed by the curves with larger decay rates.

C. Chiral atom-waveguide couplings

Light shows remarkable features when it is confined to nanophotonic structures (such as nanophotonic waveguides) on subwavelength scales. One interesting effect which appears in this context is the enhancement of the spin-orbit coupling of light [51]. As a consequence of this effect, the propagation direction of light and local spin direction may become orthogonal so that (due to time-reversal symmetry) whenever the propagation direction of light is reversed, the corresponding spin direction is also reversed. The light under discussion can be produced, for instance, by spontaneous emission from atoms or quantum dots that are evanescently coupled to nanowaveguides. Using such emitters, one can excite a transition and emit a photon with a desired spin-polarization direction. In waveguide QED, we define the chirality as the imbalance in the left and right waveguide emission directions. Along with theoretical efforts [31,52], many experiments have been performed to study chirality effects in various systems [48,51,53,54]. For instance, Mitsch *et al.* [55] have achieved more than 80% directional emission by coupling cesium atoms to silica nanofibers, exciting atoms to Zeeman states of the $6P_{3/2}$, $F = 5$ manifold. Furthermore, in photonic crystals [48] even 90% directionalities and 98% atom-waveguide coupling strengths have been achieved.

In view of these developments, in this subsection we suppose that the emission from all atoms is preferential in one direction. To this end, we take $\gamma_{iR} = 5\gamma_{iL}$, $i = 1, \ldots, 5$, while utilizing the fact that the single-photon drive is also launched towards the right in the waveguide which enhances the interaction of the first atom with its partners towards right. Note that these chiral decay rates values and $\beta \sim 1$ lies within the experimental reported values [48].

In Fig. 4(a) we plot the population dynamics. We observe that the effect of chirality is marked in contrast to the nonchiral setting shown in Fig. 2. Chirality supports better single-excitation transfer to the system. It also supports longer population trapping as the number of atoms is increased. This can be quantitatively understood by noticing that compared to the single-atom case, in the case of two, three, four, and five atoms, the maximum population attained by the system becomes 24.7%, 25.7%, 25.9%, and 26.5%, respectively. Besides the longer overall survival of a single photon in the system as a function of the number of atoms, a plateau emerges around the maximum value of the single-excitation population, becoming more pronounced as the number of atoms is increased.

As shown in Fig. 4(b), chirality also enhances entanglement. For the two-qubit case, this enhancement is more than

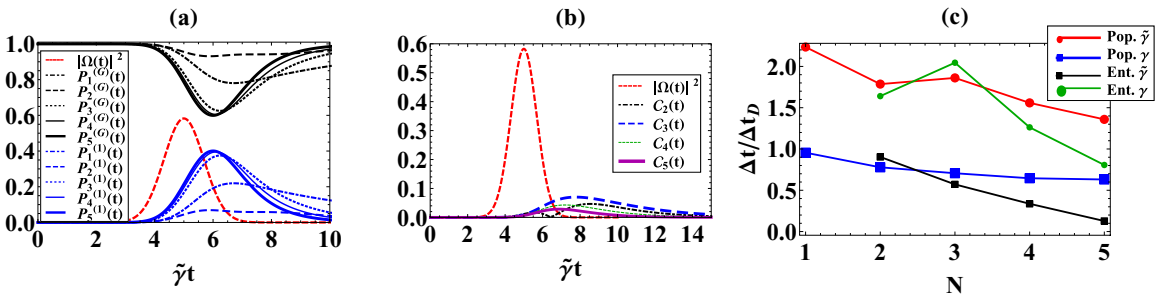

FIG. 3. Effect of small decay rates on the time evolution of (a) populations and (b) pairwise concurrence for two, three, four, and five atoms coupled to a waveguide. All parameters are the same as used in Fig. 2, except that we have chosen smaller cooperative and pure decay rates: $\tilde{\gamma}_{iL} = \tilde{\gamma}_{iR} = \tilde{\gamma}$, while $\tilde{\gamma} = 0.1\gamma$. (c) Excited-state population and entanglement survival time Δt plotted as a function of pulse-duration time Δt_D for both small decay rate $\tilde{\gamma}$ and large decay rate γ. We see that by choosing smaller decay rates, both the populations and the entanglement can be preserved for longer times.

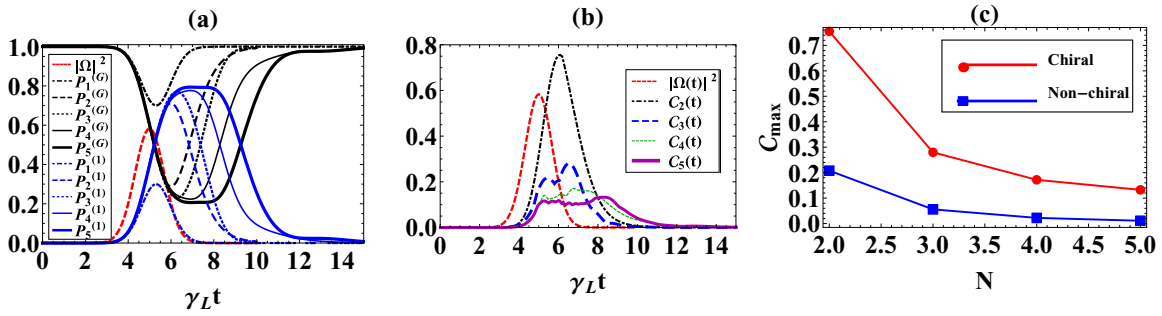

FIG. 4. Time evolution of (a) populations (b) and pairwise concurrence for a two, three, four, and five atoms coupled to a waveguide under chiral conditions. We have selected $\gamma_{1L} = \gamma_{2L} = \gamma_{3L} = \gamma_{4L} = \gamma_{5L} = \gamma_L$ (and similarly for all $\gamma_{iR}, \forall\, i = 2,3,4,5$) but $\gamma_{iR}/\gamma_{iL} = 5$. Other parameters used are as in Fig. 2. (c) Comparison of maximum entanglement $\mathcal{C}_{\max}$ achieved under the present chiral setting to the nonchiral case, both plotted as a function of the number of atoms N in the atomic chain. We see that chirality (irrespective of the number of qubits in the atomic chain) increases the maximum entanglement in the system by at least a factor of 3/2.

three times greater than the corresponding nonchiral case [see Fig. 4(c)]. For the multiqubit cases, the maximum pairwise concurrence remains 3/2 times as large as in the nonchiral case. In such multipartite situations, we also note the appearance of an oscillatory pattern in $\mathcal{C}$. Such a pattern, which eventually turns into an entanglement plateau, exhibits the fact that with a larger number of atoms in the system, a single photon transfers back and forth among qubits with unequal probability, such that the overall pairwise entanglement survives for an extended period of time.

The reason that chirality increases the maximum entanglement in the system relies on the fact that for the nonchiral case ($\gamma_{iL} = \gamma_{jL} = \gamma_{iR} = \gamma_{jR} \equiv \gamma$) the Liouvillian responsible for waveguide-mediated qubit-qubit interaction ($\hat{\mathcal{L}}_{cd}[\hat{\varrho}(t)]$) takes the form

$$\hat{\mathcal{L}}_{cd}[\hat{\varrho}(t)] = -\gamma \sum_{i\neq j=1}^{N} (\delta_{i>j} + \delta_{i<j})[\hat{\sigma}_j^\dagger \hat{\sigma}_i \hat{\varrho}(t) - \hat{\sigma}_i \hat{\varrho}(t) \hat{\sigma}_j^\dagger] + \text{H.c.}$$

It follows that the application of this Liouvillian will only contribute to real (or so-called incoherent [14,31]) terms in qubit-qubit interactions. However, in the chiral case along with the above terms, the Liouvillian also contains pure imaginary qubit-qubit interaction terms. These terms result in the availability of an additional coherent photon transfer channel among the qubits, leading to overall entanglement enhancement compared to the nonchiral setting.

D. Detuning and delays

We now suppose that the incoming single-photon is detuned from the atomic resonances; that is, ω_p is slightly mismatched from ω_{eg}. In Fig. 5(a) we present our numerical results. We notice that the detuning does not affect the overall profile of the pairwise concurrence. Moreover, as the number of atoms increases, the difference between the $\mathcal{C}_{\max}$ values attained in the detuned and on-resonance cases becomes smaller.

Next, we consider the effect of delays on entanglement. The delays we consider are introduced through the phases appearing in the atom-waveguide interaction Hamiltonian [see Eq. (A1)]. Three different phases (interatomic separations) are considered, namely, $L/\lambda_0, L/16\lambda_0$, and $L/8\lambda_0$. Even though the structure of the master equation at hand is non-Markovian, we impose the Markovian regime requirement on delays, i.e., $\gamma D \leqslant v_g$ [56,57]. In Fig. 5(b) we have plotted the quantity $\mathcal{C}(t)$, which includes the effects of delays. In the two-atom case, we observe that as we decrease the separation from L to $L/8$ (dashed black curve) and finally to $L/16$ [dotted black curve in Fig. 5(b)], the entanglement exhibits a slight enhancement. In the three-atom case, we point out that as the separation is reduced, the entanglement shows two regions of growth and decay. For $d = L/8, L/16$, the entanglement shows a partial decay after an initial growth, while later in time the entanglement decays slowly. Similarly, in the four-atom case, the smallest separation produces the largest maximum entanglement (for three atoms it is ∼0.06, while for four atoms it becomes ∼0.08). For the four-atom example, the entanglement is more than three times the maximum entanglement gained for the case of the largest separation (∼0.024). This behavior suggests that by decreasing the distance between the atoms, the width of the photonic

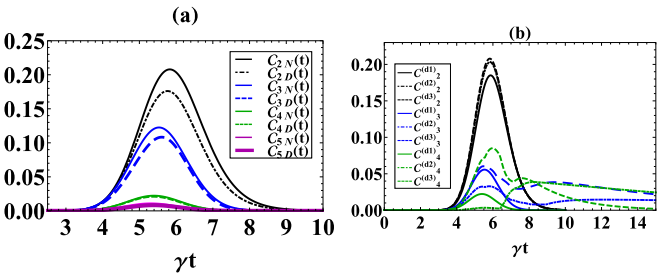

FIG. 5. (a) Finite detuning and entanglement evolution. All atoms in the chain are assumed to have the same resonant frequency ω_{eg}, which is 0.5γ detuned from ω_p. Here $\mathcal{C}_{kN}$ and $\mathcal{C}_{kD}$ are the concurrences for the no-detuning and finite-detuning cases, respectively, for $k = 2,3,4,5$. We see that detuning has a slight effect on the maximum generated entanglement. (b) Time delays between the atoms and entanglement evolution. Three different phases are plotted, namely, $d_1 = L, d_2 = L/8$, and $d_3 = L/16$ [while $D\lambda_0$ used in Eq. (3) equals d_1, d_2, and d_3]. The remaining parameters [for both (a) and (b)] are the same as in Fig. 2. We find that smaller delays support higher maximum entanglement.

wave packet emitted by the first atom becomes larger than the qubit-qubit separation. As a result, before the decay of the first qubit, the population reaches the second qubit, and from the second qubit this process extends to the third qubit and so on. Hence, the overall concurrence becomes more pronounced with an increasing number of qubits. Finally, we remark that the revival profile of the pairwise concurrence that is observed for smaller separations provides a means to probe the temporal pattern of entanglement by varying the atomic separation.

IV. CONCLUSIONS

In this paper, we have studied the manner in which a single-photon wave packet with a Gaussian spectral profile can distribute its population and stimulate entanglement among atoms in lossless waveguide QED. By applying a bidirectional single-photon Fock-state master equation, we report several findings. First, as the number of atoms increases, both the single-excitation population and the average pairwise concurrence are considerably reduced. Second, the problem of short entanglement survival time is somewhat mitigated by the utilization of small decay rates. Third, we have found that the introduction of chirality can increase the entanglement and population by more than a factor of 3/2 compared to the nonchiral case. Fourth, nonzero detuning has only a modest effect on entanglement. Inclusion of smaller delays leads to higher maximum entanglement. Finally, entanglement death and revival patterns appear which allow some control of the overall temporal profile of the entanglement. Such control is important for practical implementation of the proposed model.

ACKNOWLEDGMENTS

We thank the reviewers for their very helpful advice. This work was supported by NSF Grants No. DMR-1120923, No. DMS-1115574, and No. DMS-1108969.

APPENDIX: DERIVATION OF THE BIDIRECTIONAL SINGLE-PHOTON FOCK-STATE MASTER EQUATION

We decompose the N-system chain into N subsystems. The dissipative dynamics of the first subsystem can be described in the Heisenberg picture through the following quantum Langevin equation [58,59]:

$$\frac{d\hat{X}_1(t)}{dt}=\frac{-i}{\hbar}[\hat{X}_1(t),\hat{H}_{\rm sys1}]-[\hat{X}_1(t),\hat{c}_1^\dagger(t)]\Bigg[\sqrt{\gamma_{1R}}e^{ik_0d_1}\hat{b}_{\rm in}^{(1R)}(t)+\sqrt{\gamma_{1L}}e^{-ik_0d_1}\hat{b}_{\rm in}^{(1L)}(t)+\left(\frac{\gamma_{1R}+\gamma_{1L}}{2}\right)\hat{c}_1\Bigg]+\text{H.c.}, \tag{A1}$$

where $\hat{X}_1(t)$ and $\hat{c}_1(t)$ are arbitrary Heisenberg picture operators belonging to system 1 and H.c. stands for the Hermitian conjugate of the terms whose prefactor is the commutator $[\hat{X}_1(t),\hat{c}_1^\dagger]$. In writing this equation, we have identified two "input" operators:

$$\hat{b}_{\rm in}^{(1R)}(t)=\frac{1}{\sqrt{2\pi}}\int_{-\infty}^{\infty}\hat{b}_R(\omega_1,t_0)e^{-i\omega_1(t-t_0)}d\omega_1, \tag{A2a}$$

$$\hat{b}_{\rm in}^{(1L)}(t)=\frac{1}{\sqrt{2\pi}}\int_{-\infty}^{\infty}\hat{b}_L(\omega_2,t_0)e^{-i\omega_2(t-t_0)}d\omega_2, \tag{A2b}$$

where t_0 represents an initial time, which can be set equal to zero without loss of generality. The input operators obey the causality condition as indicated by the commutation relation: $[\hat{b}_{\rm in}^{(1\,j)}(t),\hat{b}_{\rm in}^{\dagger(1\,j)}(t')]=\delta(t-t'),\ j=R,L$. Following along the same lines, one can express the dissipative dynamics of each individual subsystem through a similar Langevin equation.

To combine the independent Langevin equations for each atom, we note that for each of the input operators appearing in Eq. (A2), there exist two output operators. For subsystem 1 these input and output operators are linked through the input-output relations [59]:

$$\hat{b}_{\rm out}^{(1R)}(t)=\hat{b}_{\rm in}^{(1R)}(t)+\sqrt{\gamma_{1R}}e^{-ik_0d_1}\hat{c}_1(t), \tag{A3a}$$

$$\hat{b}_{\rm out}^{(1L)}(t)=\hat{b}_{\rm in}^{(1L)}(t)+\sqrt{\gamma_{1L}}e^{ik_0d_1}\hat{c}_1(t), \tag{A3b}$$

where t_1 is a future time. We define the output operators as

$$\hat{b}_{\rm out}^{(1R)}(t)=\frac{1}{\sqrt{2\pi}}\int_{-\infty}^{\infty}\hat{b}_R(\omega_1,t_1)e^{-i\omega_1(t-t_1)}d\omega_1, \tag{A4a}$$

$$\hat{b}_{\rm out}^{(1L)}(t)=\frac{1}{\sqrt{2\pi}}\int_{-\infty}^{\infty}\hat{b}_L(\omega_2,t_1)e^{-i\omega_2(t-t_1)}d\omega_2. \tag{A4b}$$

Next, we note that the output from one subsystem feeds into the nearest subsystems as a time-delayed input. For instance, for just a two-subsystem example we have

$$\hat{b}_{\rm in}^{(2R)}(t)=\hat{b}_{\rm out}^{(1R)}(t-\tau)=\hat{b}_{\rm in}^{(1R)}(t-\tau)+\sqrt{\gamma_{1R}}e^{-ik_0d_1}\hat{c}_1(t-\tau), \tag{A5a}$$

$$\hat{b}_{\rm in}^{(1L)}(t)=\hat{b}_{\rm out}^{(2L)}(t-\tau)=\hat{b}_{\rm in}^{(2L)}(t-\tau)+\sqrt{\gamma_{1R}}e^{ik_0d_1}\hat{c}_2(t-\tau). \tag{A5b}$$

If we neglect the time delays, assuming that each subsystem evolves on a time scale much slower than the time a photon takes to travel between the subsystems, $\omega_{egi},\gamma_{il}\ll 1/\tau=L/c,\ l=R,L$, we arrive at the following bidirectional combined Langevin equation for an arbitrary operator $\hat{X}(t)$:

$$\frac{d\hat{X}(t)}{dt}=\frac{-i}{\hbar}[\hat{X},\hat{H}_{\rm sys}]-\sum_{i=1}^{N}\Bigg\{[\hat{X},\hat{c}_i^\dagger]\Bigg[\sqrt{\gamma_{iR}}e^{ik_0d_i}\hat{b}_{\rm in}^{(iR)}+\sqrt{\gamma_{iL}}e^{-ik_0d_i}\hat{b}_{\rm in}^{(iL)}+\left(\frac{\gamma_{iR}+\gamma_{iL}}{2}\right)\hat{c}_i+\sum_{j\neq i=1}^{N}e^{ik_0(d_i-d_j)}(\sqrt{\gamma_{iR}\gamma_{jR}}\delta_{i>j}\hat{c}_j+\sqrt{\gamma_{iL}\gamma_{jL}}\delta_{i<j}\hat{c}_j)\Bigg]+\text{H.c.}\Bigg\}. \tag{A6}$$

Here bidirectionality is manifested by terms with prefactors $\sqrt{\gamma_{il}\gamma_{jl}}$, $l = R,L$ and $\delta_{i\leqslant j} = 1$ only when $i \leqslant j$. Next, we transform to the Schrödinger picture using the identity:

$$\mathrm{Tr}_{S\oplus R}\left[\frac{d\hat{X}(t)}{dt}\hat{\rho}_s(t_0)\right] = \mathrm{Tr}_S\left[\hat{X}(t_0)\frac{d\hat{\rho}_s(t)}{dt}\right], \tag{A7}$$

where $\hat{\rho}_s(t)$ is the system reduced density matrix. Therefore, we obtain

$$\begin{aligned}\frac{d\hat{\rho}_s(t)}{dt} &= \hat{\mathcal{L}}_{cs}[\hat{\rho}_s(t)] + \hat{\mathcal{L}}_{pd}[\hat{\rho}_s(t)] + \hat{\mathcal{L}}_{cd}[\hat{\rho}_s(t)] \\ &\quad - \mathrm{Tr}_{S\oplus R}\Bigg[\sum_{i=1}^{N}\Big(\sqrt{\gamma_{iR}}\Big\{e^{ik_0d_i}[\hat{X}(t),\hat{c}_i^\dagger(t)]\hat{b}_{\mathrm{in}}^{(1R)}(t)\hat{\rho}(t_0) \\ &\quad - e^{-ik_0d_i}\hat{b}_{\mathrm{in}}^{\dagger(1R)(t)}[\hat{X}(t),\hat{c}_i(t)]\hat{\rho}(t_0)\Big\} \\ &\quad - \sqrt{\gamma_{iL}}\Big\{e^{-ik_0d_i}[\hat{X}(t),\hat{c}_i^\dagger(t)]\hat{b}_{\mathrm{in}}^{(NL)}(t)\hat{\rho}(t_0) \\ &\quad - e^{ik_0d_i}\hat{b}_{\mathrm{in}}^{\dagger(NL)(t)}[\hat{X}(t),\hat{c}_i(t)]\hat{\rho}(t_0)\Big\}\Big)\Bigg],\end{aligned} \tag{A8}$$

where $D = L/\lambda_0$. We now focus our attention on the input operator terms. We note that a considerable simplification arises from the fact that the state of the left-moving continuum is initially the vacuum. As a result, all terms involving the $\hat{b}_{\mathrm{in}}^{(NL)}(t)$ operator must vanish:

$$\begin{aligned}\mathrm{Tr}_{S\oplus R}\big\{[\hat{X}(t),\hat{c}_i^\dagger(t)]\hat{b}_{\mathrm{in}}^{(iL)}(t)\hat{\rho}(t_0)\big\} &= \mathrm{Tr}_{S\oplus R}\big\{[\hat{X}(t),\hat{c}_i^\dagger(t)] \\ &\quad \times \hat{\rho}_s(t_0)\otimes\hat{\rho}_{R1}(t_0)\otimes\hat{b}_{\mathrm{in}}^{(iL)}(t)|\mathrm{vac}\rangle\langle\mathrm{vac}|\big\} = 0,\end{aligned}$$

where we have assumed that the initial state of the global system is factorizable into system and bath initial states. Note that the right-moving continuum input terms do not vanish due to the presence of a single photon in the initial state of the reservoir.

For the single-photon wave packet in (1), we find that $\hat{b}_{\mathrm{in}}^{(iR)}(t)|\Psi_{\mathcal{R}_1}\rangle = g(t)|\mathrm{vac}\rangle$ and hence

$$\begin{aligned}\mathrm{Tr}_{S\oplus R}\{[\hat{X}(t),\hat{c}_i^\dagger]\hat{b}_{\mathrm{in}}^{(iR)}(t)\hat{\rho}(t_0)\} &= \mathrm{Tr}_{S\oplus R}\{[\hat{X}(t),\hat{c}_i^\dagger(t)] \\ &\quad \hat{\rho}_s(t_0)\otimes\hat{b}_{\mathrm{in}}^{(iR)}(t)\big|\Psi_{\mathcal{R}_1}\big\rangle\big\langle\Psi_{\mathcal{R}_1}\big|\otimes\hat{\rho}_{R2}(t_0)\} \\ &= g(t)\mathrm{Tr}_S\{\hat{X}(t_0)[\hat{c}_i^\dagger,\hat{\rho}_{01}(t)]\},\end{aligned}$$

with $g(t)$ being the temporal shape of the single-photon wave packet. The density matrix element $\hat{\rho}_{01}(t)$ is a novel and a nonphysical density operator; it follows that $\hat{\rho}_{01}^\dagger(t) = \hat{\rho}_{10}(t)$. The form of $\hat{\rho}_{10}(t)$ has already been mentioned in Sec. II B. Putting everything together, we obtain the required bidirectional single-photon Fock-state master equation,

$$\begin{aligned}\frac{d\hat{\rho}_s(t)}{dt} &= \hat{\mathcal{L}}_{cs}[\hat{\rho}_s(t)] + \hat{\mathcal{L}}_{pd}[\hat{\rho}_s(t)] + \hat{\mathcal{L}}_{cd}[\hat{\rho}_s(t)] \\ &\quad + \sum_{i=1}^{N}\sqrt{2\gamma_{iR}}\{e^{ik_0d_i}g(t)[\hat{\rho}_{01}(t),\hat{\sigma}_i^\dagger] \\ &\quad + e^{-ik_0d_i}g^*(t)[\hat{\sigma}_i,\hat{\rho}_{10}(t)]\}.\end{aligned} \tag{A9}$$

In order to obtain the equation of motion obeyed by ρ_{10}, we use the identity mentioned in (A7) to obtain

$$\mathrm{Tr}_{S\oplus R}\left[\frac{d\hat{X}(t)}{dt}\hat{\rho}_{10}(t_0)\right] = \mathrm{Tr}_S\left[\hat{X}(t_0)\frac{d\hat{\rho}_{10}(t)}{dt}\right]. \tag{A10}$$

Consequently, we find that

$$\begin{aligned}\frac{d\hat{\rho}_{10}(t)}{dt} &= \hat{\mathcal{L}}_{cs}[\hat{\rho}_{10}(t)] + \hat{\mathcal{L}}_{pd}[\hat{\rho}_{10}(t)] + \hat{\mathcal{L}}_{cd}[\hat{\rho}_{10}(t)] \\ &\quad + \sum_{i=1}^{N}\sqrt{\gamma_{iR}}e^{-ik_0d_i}g^*(t)[\hat{\rho}_{00}(t),\hat{\sigma}_i^\dagger].\end{aligned} \tag{A11}$$

Likewise, we see that $\hat{\rho}_{00}(t)$ obeys

$$\frac{d\hat{\rho}_{00}(t)}{dt} = \hat{\mathcal{L}}_{cs}[\hat{\rho}_{00}(t)] + \hat{\mathcal{L}}_{pd}[\hat{\rho}_{00}(t)] + \hat{\mathcal{L}}_{cd}[\hat{\rho}_{00}(t)]. \tag{A12}$$

[1] H. J. Kimble, The quantum Internet, Nature (London) **453**, 1023 (2008).

[2] T. D. Ladd, F. Jelezko, R. Laflamme, Y. Nakamura, C. Monroe, and J. L. O'Brien, Quantum computers, Nature (London) **464**, 45 (2010).

[3] T. E. Northup and R. Blatt, Quantum information transfer using photons, Nat. Photonics **8**, 356 (2014).

[4] H. Mabuchi and A. C. Doherty, Cavity quantum electrodynamics: Coherence in context, Science **298**, 1372 (2002).

[5] S. Haroche and D. Kleppner, Cavity quantum electrodynamics, Phys. Today **42**(1), 24 (1989).

[6] P. Bermel, A. Rodriguez, S. G. Johnson, J. D. Joannopoulos, and M. Soljačić, Single-photon all-optical switching using waveguide-cavity quantum electrodynamics, Phys. Rev. A **74**, 043818 (2006).

[7] H. Zheng, D. J. Gauthier, and H. U. Baranger, Waveguide-QED-Based Photonic Quantum Computation, Phys. Rev. Lett. **111**, 090502 (2013).

[8] A. Akimov, A. Mukherjee, C. Yu, D. Chang, A. Zibrov, P. Hemmer, H. Park, and M. Lukin, Generation of single optical plasmons in metallic nanowires coupled to quantum dots, Nature (London) **450**, 402 (2007).

[9] A. Goban, C.-L. Hung, S.-P. Yu, J. Hood, J. Muniz, J. Lee, M. Martin, A. McClung, K. Choi, D. Chang *et al.*, Atom-light interactions in photonic crystals, Nat. Commun. **5**, 3808 (2014).

[10] D. E. Chang, J. I. Cirac, and H. J. Kimble, Self-Organization of Atoms along a Nanophotonic Waveguide, Phys. Rev. Lett. **110**, 113606 (2013).

[11] C. Rigetti, J. M. Gambetta, S. Poletto, B. Plourde, J. M. Chow, A. Córcoles, J. A. Smolin, S. T. Merkel, J. Rozen, G. A. Keefe *et al.*, Superconducting qubit in a waveguide cavity with a coherence time approaching 0.1 ms, Phys. Rev. B **86**, 100506 (2012).

[12] J.-B. Béguin, E. M. Bookjans, S. L. Christensen, H. L. Sørensen, J. H. Müller, E. S. Polzik, and J. Appel, Generation and Detection of a Sub-Poissonian Atom Number Distribution in a One-Dimensional Optical Lattice, Phys. Rev. Lett. **113**, 263603 (2014).

[13] H. Zheng and H. U. Baranger, Persistent Quantum Beats and Long-Distance Entanglement from Waveguide-Mediated Interactions, Phys. Rev. Lett. **110**, 113601 (2013).
[14] C. Gonzalez-Ballestero, A. Gonzalez-Tudela, F. J. Garcia-Vidal, and E. Moreno, Chiral route to spontaneous entanglement generation, Phys. Rev. B **92**, 155304 (2015).
[15] A. Gonzalez-Tudela, D. Martin-Cano, E. Moreno, L. Martin-Moreno, C. Tejedor, and F. J. Garcia-Vidal, Entanglement of Two Qubits Mediated by One-Dimensional Plasmonic Waveguides, Phys. Rev. Lett. **106**, 020501 (2011).
[16] C. Y. Hu, A. Young, J. L. O'Brien, W. J. Munro, and J. G. Rarity, Giant optical Faraday rotation induced by a single-electron spin in a quantum dot: Applications to entangling remote spins via a single photon, Phys. Rev. B **78**, 085307 (2008).
[17] J.-H. An, M. Feng, and C. H. Oh, Quantum-information processing with a single photon by an input-output process with respect to low-Q cavities, Phys. Rev. A **79**, 032303 (2009).
[18] A. González-Tudela and D. Porras, Mesoscopic Entanglement Induced by Spontaneous Emission in Solid-State Quantum Optics, Phys. Rev. Lett. **110**, 080502 (2013).
[19] C. Aron, M. Kulkarni, and H. E. Türeci, Steady-state entanglement of spatially separated qubits via quantum bath engineering, Phys. Rev. A **90**, 062305 (2014).
[20] J. M. Fink, R. Bianchetti, M. Baur, M. Göppl, L. Steffen, S. Filipp, P. J. Leek, A. Blais, and A. Wallraff, Dressed Collective Qubit States and the Tavis-Cummings Model in Circuit QED, Phys. Rev. Lett. **103**, 083601 (2009).
[21] Y. Zhang, L. Yu, J.-Q. Liang, G. Chen, S. Jia, and F. Nori, Quantum phases in circuit QED with a superconducting qubit array, Sci. Rep. **4**, 4083 (2014).
[22] J.-T. Shen and S. Fan, Theory of single-photon transport in a single-mode waveguide. I. Coupling to a cavity containing a two-level atom, Phys. Rev. A **79**, 023837 (2009).
[23] S. Fan, Ş. E. Kocabaş, and J.-T. Shen, Input-output formalism for few-photon transport in one-dimensional nanophotonic waveguides coupled to a qubit, Phys. Rev. A **82**, 063821 (2010).
[24] T. Caneva, M. T. Manzoni, T. Shi, J. S. Douglas, J. I. Cirac, and D. E. Chang, Quantum dynamics of propagating photons with strong interactions: A generalized input-output formalism, New J. Phys. **17**, 113001 (2015).
[25] T. Shi, D. E. Chang, and J. I. Cirac, Multiphoton-scattering theory and generalized master equations, Phys. Rev. A **92**, 053834 (2015).
[26] H. Zoubi, Collective interactions in an array of atoms coupled to a nanophotonic waveguide, Phys. Rev. A **89**, 043831 (2014).
[27] M. Arcari, I. Söllner, A. Javadi, S. L. Hansen, S. Mahmoodian, J. Liu, H. Thyrrestrup, E. H. Lee, J. D. Song, S. Stobbe *et al.*, Near-Unity Coupling Efficiency of a Quantum Emitter to a Photonic Crystal Waveguide, Phys. Rev. Lett. **113**, 093603 (2014).
[28] K.-M. Fu, C. Santori, P. Barclay, I. Aharonovich, S. Prawer, N. Meyer, A. Holm, and R. Beausoleil, Coupling of nitrogen-vacancy centers in diamond to a gap waveguide, Appl. Phys. Lett. **93**, 234107 (2008).
[29] K. Lalumière, B. C. Sanders, A. F. van Loo, A. Fedorov, A. Wallraff, and A. Blais, Input-output theory for waveguide QED with an ensemble of inhomogeneous atoms, Phys. Rev. A **88**, 043806 (2013).
[30] R. H. Lehmberg, Radiation from an N-atom system. I. General formalism, Phys. Rev. A **2**, 883 (1970).
[31] H. Pichler, T. Ramos, A. J. Daley, and P. Zoller, Quantum optics of chiral spin networks, Phys. Rev. A **91**, 042116 (2015).
[32] J.-H. An and W.-M. Zhang, Non-Markovian entanglement dynamics of noisy continuous-variable quantum channels, Phys. Rev. A **76**, 042127 (2007).
[33] Q.-J. Tong, J.-H. An, H.-G. Luo, and C. H. Oh, Mechanism of entanglement preservation, Phys. Rev. A **81**, 052330 (2010).
[34] B. Q. Baragiola, R. L. Cook, A. M. Brańczyk, and J. Combes, N-photon wave packets interacting with an arbitrary quantum system, Phys. Rev. A **86**, 013811 (2012).
[35] K. M. Gheri, K. Ellinger, T. Pellizari, and P. Zoller, Photon-wavepackets as flying quantum bits, Fortschr. Phys. **46**, 401 (1998).
[36] W. K. Wootters, Entanglement of Formation of an Arbitrary State of Two Qubits, Phys. Rev. Lett. **80**, 2245 (1998).
[37] L. Amico, R. Fazio, A. Osterloh, and V. Vedral, Entanglement in many-body systems, Rev. Mod. Phys. **80**, 517 (2008).
[38] M. Yönaç, T. Yu, and J. Eberly, Pairwise concurrence dynamics: A four-qubit model, J. Phys. B **40**, S45 (2007).
[39] X. Wang, S. Ghose, B. C. Sanders, and B. Hu, Entanglement as a signature of quantum chaos, Phys. Rev. E **70**, 016217 (2004).
[40] M. Sarovar, A. Ishizaki, G. R. Fleming, and K. B. Whaley, Quantum entanglement in photosynthetic light-harvesting complexes, Nat. Phys. **6**, 462 (2010).
[41] X. Wang and B. C. Sanders, Spin squeezing and pairwise entanglement for symmetric multiqubit states, Phys. Rev. A **68**, 012101 (2003).
[42] Y. Wang, J. Minář, L. Sheridan, and V. Scarani, Efficient excitation of a two-level atom by a single photon in a propagating mode, Phys. Rev. A **83**, 063842 (2011).
[43] C. Clausen, I. Usmani, F. Bussières, N. Sangouard, M. Afzelius, H. de Riedmatten, and N. Gisin, Quantum storage of photonic entanglement in a crystal, Nature (London) **469**, 508 (2011).
[44] E. Saglamyurek, J. Jin, V. B. Verma, M. D. Shaw, F. Marsili, S. W. Nam, D. Oblak, and W. Tittel, Quantum storage of entangled telecom-wavelength photons in an erbium-doped optical fibre, Nat. Photonics **9**, 83 (2015).
[45] D.-S. Ding, W. Zhang, Z.-Y. Zhou, S. Shi, G.-Y. Xiang, X.-S. Wang, Y.-K. Jiang, B.-S. Shi, and G.-C. Guo, Quantum Storage of Orbital Angular Momentum Entanglement in an Atomic Ensemble, Phys. Rev. Lett. **114**, 050502 (2015).
[46] S. Fedortchenko, A. Keller, T. Coudreau, and P. Milman, Finite-temperature reservoir engineering and entanglement dynamics, Phys. Rev. A **90**, 042103 (2014).
[47] S. G. Schirmer and X. Wang, Stabilizing open quantum systems by Markovian reservoir engineering, Phys. Rev. A **81**, 062306 (2010).
[48] I. Söllner, S. Mahmoodian, S. L. Hansen, L. Midolo, A. Javadi, G. Kiršanskė, T. Pregnolato, H. El-Ella, E. H. Lee, J. D. Song *et al.*, Deterministic photon-emitter coupling in chiral photonic circuits, Nat. Nanotechnol. **10**, 775 (2015).
[49] L. Mazzola, S. Maniscalco, J. Piilo, K.-A. Suominen, and B. M. Garraway, Sudden death and sudden birth of entanglement in common structured reservoirs, Phys. Rev. A **79**, 042302 (2009).

[50] J.-S. Xu, C.-F. Li, M. Gong, X.-B. Zou, C.-H. Shi, G. Chen, and G.-C. Guo, Experimental Demonstration of Photonic Entanglement Collapse and Revival, Phys. Rev. Lett. **104**, 100502 (2010).

[51] J. Petersen, J. Volz, and A. Rauschenbeutel, Chiral nanophotonic waveguide interface based on spin-orbit interaction of light, Science **346**, 67 (2014).

[52] T. Ramos, H. Pichler, A. J. Daley, and P. Zoller, Quantum Spin Dimers from Chiral Dissipation in Cold-Atom Chains, Phys. Rev. Lett. **113**, 237203 (2014).

[53] F. Le Kien and A. Rauschenbeutel, Anisotropy in scattering of light from an atom into the guided modes of a nanofiber, Phys. Rev. A **90**, 023805 (2014).

[54] R. J. Coles, D. M. Price, J. E. Dixon, B. Royall, E. Clarke, P. Kok, M. S. Skolnick, A. M. Fox, and M. N. Makhonin, Chirality of nanophotonic waveguide with embedded quantum emitter for unidirectional spin transfer, Nat. Commun. **7**, 11183 (2016).

[55] R. Mitsch, C. Sayrin, B. Albrecht, P. Schneeweiss, and A. Rauschenbeutel, Quantum state-controlled directional spontaneous emission of photons into a nanophotonic waveguide, Nat. Commun. **5**, 5713 (2014).

[56] Y.-L. L. Fang and H. U. Baranger, Waveguide QED: Power spectra and correlations of two photons scattered off multiple distant qubits and a mirror, Phys. Rev. A **91**, 053845 (2015).

[57] T. Tufarelli, M. S. Kim, and F. Ciccarello, Non-Markovianity of a quantum emitter in front of a mirror, Phys. Rev. A **90**, 012113 (2014).

[58] U. Weiss, *Quantum Dissipative Systems* (World Scientific, Singapore, 1999).

[59] C. Gardiner and P. Zoller, *Quantum Noise: A Handbook of Markovian and Non-Markovian Quantum Stochastic Methods with Applications to Quantum Optics* (Springer, Berlin, 2004).